Title

Aifm2, a NADH Oxidase, Supports Robust Glycolysis and Is Required for Cold- and Diet-Induced Thermogenesis

Journal

Molecular Cell, 77(3)

ISSN

1097-2765

Authors

Nguyen, Hai P
Yi, Danielle
Lin, Frances
et al.

Publication Date

2020-02-01

DOI

10.1016/j.molcel.2019.12.002

Peer reviewed

HHS Public Access

Author manuscript

Mol Cell. Author manuscript; available in PMC 2021 February 06.

Published in final edited form as:

Mol Cell. 2020 February 06; 77(3): 600–617.e4. doi:10.1016/j.molcel.2019.12.002.

Aifm2, a NADH oxidase, supports robust glycolysis and is required for cold- and diet-induced thermogenesis

Hai P. Nguyen[1,2], **Danielle Yi**[1,2], **Frances Lin**[2], **Jose A. Viscarra**[2], **Chihiro Tabuchi**[2], **Katina Ngo**[2], **Gawon Shin**[2], **Angus Yiu-fai Lee**[3], **Yuhui Wang**[2], **Hei Sook Sul**[1,2,4,*]

[1]Endocrinology Program

[2]Department of Nutritional Sciences & Toxicology, University of California, Berkeley, CA, USA

[3]Department of Molecular and Cell Biology, University of California, Berkeley, CA, USA

[4]Lead contact

SUMMARY

Brown adipose tissue (BAT) is highly metabolically active tissue to dissipate energy via UCP1 as heat, and BAT mass is correlated negatively with obesity. The presence of BAT/BAT-like tissue in humans renders BAT as attractive target against obesity and insulin resistance. Here, we identify Aifm2, a NADH oxidoreductase domain containing flavoprotein, as a lipid droplet (LD) associated protein highly enriched in BAT. Aifm2 is induced by cold, as well as by diet. Upon cold or β-adrenergic stimulation, Aifm2 associates with the outer side of the mitochondrial inner membrane. As a unique BAT-specific first mammalian NDE (external NADH dehydrogenase)-like enzyme, Aifm2 oxidizes NADH to maintain high cytosolic NAD levels in supporting robust glycolysis and to transfer electrons to ETC for fueling thermogenesis. Aifm2 in BAT and subcutaneous WAT promotes oxygen consumption, uncoupled respiration and heat production during cold- and diet-induced thermogenesis. Aifm2, thus, can ameliorate diet-induced obesity and insulin resistance.

ETOC blurb:

Aifm2, a brown adipose tissue specific lipid-droplet associated NADH oxidase, associates with mitochondrial inner membrane to regenerate cytosolic NAD for robust glycolysis and to support ETC for thermogenesis.

Graphical Abstract

*Correspondence: hsul@berkeley.edu.

AUTHOR CONTRIBUTIONS

H.N. performed the initial screen, loss/gain-of function studies *in vitro*, and characterized mouse models. D.Y. assisted in Seahorse and CLAMS. F.L. and K.N. assisted in RT-qPCR and animal studies. J.V. constructed Aifm2 plasmids. C.T. assisted animal studies. A.Y.L assisted in creating mouse models. Y.W. provided guidance for experiments. H.S.S. designed the project, guided experiments and analysis of data. H.N., D.Y., H.S.S. wrote and edited the manuscript.

DECLARATION OF INTERESTS

The authors declare no competing interests.

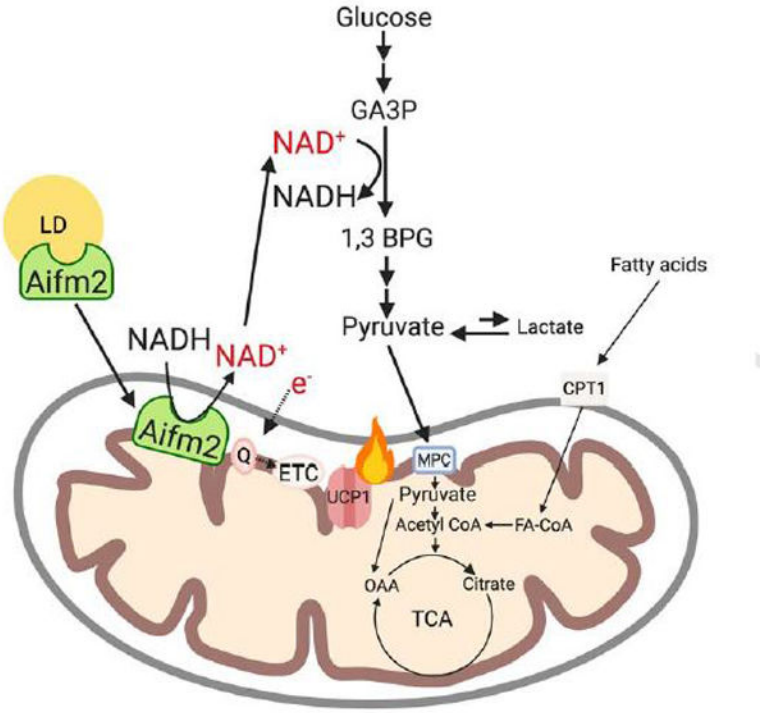

INTRODUCTION

Obesity, characterized by the excess accumulation of white adipose tissue (WAT), has become a global epidemic. In contrast to WAT that serves as the main energy storage organ, brown adipose tissue (BAT) dissipates energy via non-shivering thermogenesis to maintain body temperature in cold. Upon cold exposure, subcutaneous WAT also becomes BAT-like via so-called browning or beiging (Bartelt and Heeren, 2014). Presence of BAT and BAT-like tissue in human adults has been established and BAT activity is known to increase upon cold exposure to inversely correlate with adiposity (Cypess et al., 2009, Virtanen et al., 2009, Nedergaard et al., 2010, van Marken Lichtenbelt et al., 2009, Carpentier et al., 2018). Unlike WAT with unilocular lipid droplet (LD), brown adipocytes contain numerous small LDs and a high number of mitochondria. Although it may not be an exclusive mechanism, UCP1 at the inner mitochondrial membrane of BAT dissipates proton gradient from mitochondrial electron transport chain (ETC) to generate heat (Cannon and Nedergaard, 2004). BAT is reported also to dissipate heat in response to diet or food intake, diet-induced thermogenesis. At thermoneutrality (30^{o}C), UCP1 KO mice are heavier. UCP1 has been shown to increase from consuming obesogenic diets (Feldmann et al., 2009). Better understanding regulation of BAT metabolism and thermogenic process may provide future therapeutic targets for obesity and related metabolic diseases.

Thermogenesis is a highly energetic process and, classically, FAs derived from intracellular lipolysis are used as the energy source (Blondin et al., 2017). Upon cold, norepinephrine released from the sympathetic innervation in BAT stimulates β_3-adrenergic receptor increasing intracellular lipolysis (Ahmadian et al., 2011). FAs thus generated are utilized for

oxidation and to directly bind for UCP1 activation (Carpentier et al., 2018). Recently, however, FAs taken up from circulation are shown to be used for thermogenesis, especially in fasted condition (Schreiber et al., 2017, Shin et al., 2017). And glucose uptake increases in BAT after cold exposure or β-adrenergic stimulation (M et al., 2018, Symonds et al., 2018). Proteins/enzymes involved in glucose uptake and catabolism, such as Glut1 and Hexokinase, are induced in BAT by cold exposure (Winther et al., 2018). BAT has the highest glucose uptake among tissues and. In fact, the presence of BAT or BAT-like tissue in adults has been evidenced by the ^{18}F-glucose uptake of PET-CT scan (M et al., 2018). Interestingly, glycolysis is reported to be critical for optogenetically induced thermogenesis (Jeong et al., 2018). Yet, neither the role nor the significance of glycolysis and its downstream metabolism during thermogenesis have been well studied.

To sustain robust glycolysis, cytosolic NAD is critical to support glyceraldehyde-3phosphate dehydrogenase reaction in the glycolytic pathway (Barron et al., 1998). Inner mitochondrial membrane is impermeable to NADH or NAD. In most tissues, malate-aspartate shuttle transfers NADH produced from glycolysis into mitochondria for ETC and returns NAD to cytosol for glycolysis. In BAT that requires rapid ATP generation, glycerol-3-phosphate shuttle is presumed critical (Kauppinen et al., 1987, Barron et al., 1998). However, contribution of mtGPD in thermogenesis could not be demonstrated in KO mouse models (DosSantos et al., 2003, Alfadda et al., 2004). Lactate dehydrogenase (LDH) reaction in the cytosol can regenerate NAD. However, lactate in BAT can be used for oxidation by converting back to pyruvate to enter TCA cycle, and lactate levels in BAT do not increase but rather decrease during thermogenesis (Jeong et al., 2018) (Vergnes and Reue, 2014). Therefore, BAT may have a unique, yet to be identified means of NAD generation for glycolysis.

NDHs (NADH dehydrogenase) that are mainly found in yeast, bacteria and plants are associated with the mitochondrial inner membrane and catalyze the same NADH oxidase reaction as complex I in ETC (Yamashita et al., 2018). There are two main classes of NDHs, NDI (internal NDH) facing the mitochondrial matrix and NDE (external) facing the intermembrane space (Iwata et al., 2012). Yeast lacks complex 1, NDI maintains mitochondrial NAD to ensure efficient TCA cycle, while NDE provides cytosolic NAD for glycolysis. NDHs increase ETC activity by transferring electrons to CoQ (Melo et al., 2004, Luttik et al., 1998a). In fact, upon environmental cues, NDE has been shown to have much higher turnover numbers of NADH:UQ oxidase activity than mammalian complex I (Elguindy and Nakamaru-Ogiso, 2015). There has been no NDHs reported in the mammalian system.

We recently have discovered that Aifm2 (Apoptosis inducing mitochondrion associated factor 2 (also called AMID, or Prg3), a flavoprotein with a NADH/NAD oxidoreductase domain as a lipid-droplet associated protein that is highly and specifically expressed in BAT and is induced upon cold exposure/β -adrenergic stimulation in BAT and iWAT. Although Aifm2 was previously reported to a be a p53 target to promote caspase-independent cell death (Marshall et al., 2005, Ohiro et al., 2002), we found Aifm2 cannot induce apoptosis in BAT cells. Upon stimulation, Aifm2 localizes to mitochondria for conversion of NADH to NAD to sustain robust glycolysis, while transferring electrons to mitochondrial ETC to fuel

thermogenesis. Remarkably, Yeast NDE1 can rescue impaired thermogenesis from Aifm2 deficiency, making Aifm2 to be a mammalian NDE specific to thermogenic tissues. GWAS database reveals multiple SNPs of Aifm2 to be associated with waist-hip ratio, body mass index and fasting glucose level-related insulin resistance, suggesting a potential role of Aifm2 in human obesity and type 2 diabetes (Dupuis et al., 2010, Speliotes et al., 2010, Heid et al., 2010).

RESULTS

Aifm2 is expressed specifically in BAT and is induced by cold.

Differ from a unilocular LD of white adipocytes, brown adipocytes contain multiple small lipid droplets (Betz and Enerbäck, 2017). In an attempt to identify BAT-specific proteins associated with smaller LDs, we isolated LD fraction from perigonadal WAT (pWAT) or BAT from mice for proteomic mass spectrometry (Harris et al., 2012). Proteins from LD fraction of adipose depots were analyzed by LC/MS. We discovered Aifm2 as a lipid droplet associated protein highly enriched only in BAT (Fig. S1A–B). Aifm2 did not possess signal sequence but contained N-terminal hydrophobic/membrane domain (aa1–27), NADH oxidoreductase domain (aa81–285) and FAD domain (aa286–308) (Fig. 1A). RT-qPCR of various mouse tissues and human tissue cDNA array revealed that Aifm2 is the highest in mouse BAT, 60-fold higher than mouse iWAT or human subcutaneous fat. Similarly, immunoblotting for Aifm2 showed Aifm2 to be highest in mouse BAT and very low level in both mouse iWAT and human subcutaneous fat, but undetectable in other tissues (Fig. 1B). In addition, databases for mice and human tissues showed Aifm2 expression to be mainly in BAT in mice and in WAT in humans (BAT not included) (Fig. S1C–D). Microarray data comparing mRNA levels in human neck BAT and WAT of 10 patients showed 10-fold higher Aifm2 mRNA levels in BAT compared to WAT. In addition, RNA seq of human neck WAT and BAT revealed Aifm2 to be positively correlated with UCP1 mRNA levels, significantly higher in BAT than WAT (Fig. 1C) (Virtanen et al., 2009). In mouse BAT, Aifm2 mRNA was 7-fold higher in adipocytes than stromal vascular fraction (SVF) (Fig. 1D). During brown adipocyte differentiation, Aifm2 mRNA was markedly increased, 7-fold higher at Day 3 than Day 0 (Fig. 1E, left). Similarly, Aifm2 protein was significantly increased during differentiation (Fig. 1E, right).

We next examined whether Aifm2 might be induced during thermogenesis. Mice were kept at either 30^{o}C or at 4^{o}C for 3 hrs. Similar to UCP1, Aifm2 mRNA levels in BAT and iWAT were greatly increased after cold exposure by 9- and 25-fold, respectively. Aifm2 protein levels in BAT and iWAT of the cold exposed mice were also higher (Fig. 1F). When mice were injected with a β3-agonist, CL-31,248, Aifm2 mRNA was increased by 12- and 4-fold, respectively in iWAT and BAT. Aifm2 protein was also increased (Fig. 1G). We identified a CRE located at −442 bp upstream of the Aifm2 start site. Co-transfecting CREB with −1500 bp Aifm2 promoter-luciferase construct resulted in a 4-fold increase in the Aifm2 promoter activity (Fig. 1H). Overall, the data demonstrate that Aifm2 is highly expressed in BAT and increases during brown adipogenesis and is induced in BAT and iWAT upon cold/β3 agonist.

Aifm2 translocates to mitochondria upon cold exposure/β-adrenergic stimulation

To examine intracellular localization of Aifm2, we first tested the presence of Aifm2 in LD of differentiated BAT cells by immunoblotting. Supernatant from lysates of BAT cells was subjected to sucrose step gradient centrifugation of 60, 20 and 5%. The top floating layer was collected as LD (Harris et al., 2012). In the basal, Aifm2 was detected at a high level in LD but also at a very low level in 5–20% fraction composed of mainly cytosolic fraction with some mitochondrial contamination as detected by low level of Tom20 (Fig. 2A, left). We further separated cytosolic fraction without mitochondrial contamination by classic differential centrifugation. Aifm2 was undetectable in the cytosolic fraction and was detected at low level in the mitochondrial fraction (Fig. 2A, right). Thus, in the basal, Aifm2 is present mainly in LD. When BAT cells were treated with CL-316,248, Aifm2 was no longer detectable in LD, but was mainly found in the mitochondrial fraction (Fig. 2A, right). Similarly, Aifm2 in BAT from mice at 30ºC was detected at a high level in LD, and at a very low level in mitochondrial fraction. In contrast, Aifm2 from mice of mice that were cold-exposed was barely detectable in LD, but was found mainly in mitochondrial fraction (Fig. 2B).

We next attempted to visualize Aifm2 in live cells. GFP-tagged Aifm2 lentivirus was transduced into differentiated BAT cells. Immunofluorescence imaging showed that Aifm2 was detected around LDs as evidenced by colocalization of GFP with LipidTox or Mitotracker Red. GFP was also detected as punctates in the cytoplasm, an indication of potential mitochondrial association of Aifm2 (Fig. 2C, left). However, with the isoproterenol (ISO), Aifm2 was no longer localized around LDs, but detected only as cytoplasmic punctates (Fig. 2C, left). GFP and lipidTox colocalization showed approximately 95% Aifm2 GFP signal surrounding lipid droplets in the basal condition. In contrast, Aifm2-GFP and lipidTox colocalization was reduced approximately to 21% upon ISO. When visualizing the Aifm2-GFP with Mitotracker Red, Aifm2GFP was mainly detected in ring-shaped structures assuming LDs in control cells. Upon ISO treatment, Aifm2-GFP was colocalized completely with Mitotracker Red (Fig. 2C, right). GFP signal and Mitotracker Red colocalization was approximately 8% in the control cells, while it increased to 87% in ISO treated cells. Overall, these results point toward translocation of Aifm2 from LD to mitochondria in BAT upon cold or β-adrenergic stimulation.

Next to identify the domains that are responsible for Aifm2 association with LDs and mitochondria, multiple Aifm2 deletion and mutation constructs were generated and expressed in differentiated BAT cells. Deletion constructs of Aifm2 N-terminal hydrophobic region aa1–27 (Aifm2 ΔN) and C-terminal aa308–373 (Aifm2 ΔC) were tagged with GFP. Since Aifm2 has been found to be myristoylated at the N-terminal a-amino group of glycine residue, Aifm2 G2A was also created by site-directed mutagenesis (Suzuki et al., 2010). Immunoblotting for Aifm2 revealed that Aifm2 G2A was present mainly in the mitochondrial fraction in the basal condition. Whereas Aifm2ΔN was found in cytosolic fraction. Similar to Aifm2 WT, Aifm2ΔC was detected mainly in the LD fraction (Fig. 2D, top). Similarly, GFP-fusion Aifm2 G2A mutant was detected as punctates that were co-stained with MitoTracker Red, but not with LipidTox (Fig. 2D, bottom left), indicating mitochondrial localization. Moreover, whereas Aifm2 ΔC-GFP did not affect Aifm2

localization, Aifm2 ΔN-GFP was detected mainly in the cytosol (Fig. 2D, bottom right). Taken together, N-terminal domain is required for both LD and mitochondrial localization and Nmyristoylation is essential for LD association of Aifm2.

To further investigate localization of Aifm2 in the mitochondria, we prepared the mitoplasts stripped of outer mitochondrial membrane from BAT cells by ultracentrifugation of digitonin-treated mitochondria. Mitoplast pellet and the supernatant containing solubilized mitochondrial outer membrane and intermembrane space (OM+IMS) were collected. In the basal condition, we could not detect Aifm2 in either mitoplasts or OM+IMS fraction. However, Aifm2 of BAT cells treated with CL-316,248 appeared highly in the mitoplast fraction but was absent in the OM+IMS fraction (Fig. 2E, left). In BAT from mice maintained at 30^{o}C, Aifm2 was present at a very low level in mitoplasts, which was increased significantly in mitoplasts from BAT of cold-exposed mice (Fig. 2E, right). Aifm2 was not detected in the OM+IMS fraction in mice maintained either at thermoneutrality or cold-exposed. We conclude that, even without mitochondrial targeting signal sequence, Aifm2 can be found in mitoplasts upon cold exposure and thus probably associated with outer side of the inner mitochondrial membrane.

Next, we compared NADH oxidase activity in various subcellular compartments to correlate with Aifm2 localization. HEK293 cells, expressing low endogenous Aifm2 were transfected with Aifm2, then treated with oleate (Fig. 2F, left). HEK293 cells are known to respond to ISO to increase cAMP due to endogenous β-receptor (Schmitt and Stork, 2000). We employed the cytosolic fraction containing LDs and intact mitoplasts and OM+IMS, to measure NADH oxidase activity by monitoring the remaining NADH levels at 340 nm using NADH as substrate. The reaction was started by adding the enzyme-containing samples preincubated with FAD. In basal condition, NADH oxidase activity in cytosolic fraction of Aifm2 OE cells was higher by 9-fold compared to control cells. NADH oxidase activity of intact mitoplasts representing that of outer side of mitoplasts, was greatly lower in Aifm2 transfected control cells (Fig. 2F). After ISO, NADH oxidase activity in mitoplasts of Aifm2 transfected cells was higher by 10-fold compared to control cells. NADH oxidase activity of solubilized mitoplasts increased by only 1.5-fold, probably due to the presence of high NADH oxidase activity from complex I and III of ETC (Data not shown). The very low NADH oxidase activity detected in the cytosolic fraction remained unchanged between transfected and control cells (Fig. 2F). These results indicate that NADH oxidase activity of cytosolic and intact mitoplast fraction is mainly from Aifm2 and that Aifm2 resides in LD in basal condition and, upon β-AR stimulation or cold-exposure, it associates with mitochondrial inner membrane facing the intermembrane space, where it oxidizes NADH to NAD.

Aifm2 maintains NAD to support glycolysis in BAT cells during thermogenesis

BAT recently has been proposed to be metabolically flexible to use not only FAs but also glucose (Iwen et al., 2017). We propose that glucose may serve as the main fuel source for thermogenesis, especially in the fed condition with high circulating glucose. To sustain robust glycolysis, BAT must maintain a NAD pool in the cytoplasm. We thus investigated whether Aifm2, with its NADH oxidase activity, affects cellular NAD/NADH by Aifm2

loss- and gain-of function experiments. To measure NAD/NADH levels, we used a biochemical assay based on lactate dehydrogenase cycling. BAT cells were treated with either control shRNA or Aifm2 pooled shRNA lentivirus. In the control, NAD/NADH ratio increased 3-fold by ISO. Aifm2 KD in BAT cells reduced NAD/NADH by 20% compared to control cells. Importantly, Aifm2 KD prevented the increase in NAD/NADH upon β-AR stimulation (Fig. 3A). Conversely, when Histagged Aifm2 was overexpressed BAT cells, NAD/NADH was increased by approximately 30%. In response to ISO, the NAD/NADH further increased by 2.5-fold (Fig. 3B). To determine intracellular compartment-specific NAD/NADH, we next documented changes in NAD/NADH in situ. We co-expressed Aifm2 with cytoplasmic Peredox, a fluorescent biosensor of NADH/NAD redox state, in HEK293 cells (Hung et al., 2011). Indeed, cytoplasmic NADH/NAD state was reduced upon ISO (Fig. 3C, left). Aifm2 overexpression (OE) decreased cytosolic NADH/NAD by 2-fold, and further decreased by 3-fold upon ISO (Fig. 3C, left). There was a slight but significant increase in NAD/NADH in control cells by ISO treatment. Moreover, NAD/NADH, which was increased 2-fold in Aifm2 OE cells, further increased by 3-fold upon β-AR stimulation (Fig. 3C, right). Overall, these results indicate that Aifm2 increases cytosolic NAD levels in BAT cells.

We next investigated whether the changes in NAD levels or NAD/NADH ratio by Aifm2 affect glycolytic rate in BAT cells. We performed extracellular acidification rate (ECAR). ECAR mainly represents glycolytic flux to lactate. ECAR in the presence of a F1/F0 ATP synthase inhibitor, oligomycin, renders maximal glycolytic capacity, due to suppression of mitochondrial ATP production, whereas addition of a hexokinase inhibitor, 2-DG blocks glucose utilization through glycolysis. ECAR in the control BAT cells showed that glycolytic rate and maximal glycolytic capacity were increased by 25% and 40%, respectively, upon ISO, whereas Aifm2 KD reduced both fluxes by approximately 25%. Aifm2 KD cells failed to increase glycolytic rate or maximal glycolytic capacity by ISO (Fig. 3D, left). Conversely, overexpression of Aifm2 significantly increased both by 25% relative to control cells. With β-AR stimulation, Aifm2 OE BAT cells further increased glycolytic rate and maximal glycolytic capacity by 25% and 40%, respectively (Fig. 3E, left). Since ECAR can be affected by CO_2 generated by TCA cycle, we also measured intracellular lactate levels. Similar to ECAR, control cells had a 3-fold increase in lactate levels with ISO. Aifm2 KD reduced lactate levels by 25%. Moreover, Aifm2 KD prevented the increase in lactate level by β-AR stimulation (Fig. 3D, right). Conversely, Aifm2 OE increased intracellular lactate levels by 25% relative to control cells. With ISO, the lactate levels were further increased by 7-fold in these Aifm2 OE BAT cells (Fig. 3E, right). The changes in lactate levels by Aifm2 KD or overexpression were larger than ECAR, which may be due to the fact that intracellular lactate reflects only a direct product of glycolysis, whereas ECAR measures lactate other acidic substrates secreted into the media. Regardless, results from using both methods clearly demonstrate the Aifm2 effect on glycolysis in BAT cells. We also tested whether Aifm2 KD also affected glycolysis in white fat cell. Aifm2 shRNA was transduced in differentiated 3T3-L1 adipocytes which has very low Aifm2 expression and the results showed no significant decrease in either glycolysis or oxygen consumption rate (OCR) in these cells (Fig. S3A–Fig. S3AB). We conclude that, with its

NADH oxidase activity, Aifm2 generates a NAD pool that allows BAT to maintain high rate of glycolysis.

Aifm2 is required for glycolysis in BAT during thermogenesis

Next, we investigated whether glycolysis promoted by Aifm2 supports thermogenesis in BAT cells. First, we measured mitochondrial membrane depolarization, which has been correlated with thermogenesis (Reers et al., 1995). In measuring mitochondrial potential, we employed a metachromatic dye-based JC-1 fluorescence probe in live cells (Salvioli et al., 1997). In polarized mitochondria, JC-1 aggregates in the mitochondrial matrix to emit light in the orange/red region, whereas in depolarized mitochondria, JC-1 monomer leaks into the cytosol to display green fluorescence. BAT cells were treated with 2 μm JC-1 for 20 mins prior to FACS analysis. In control cells, ISO treatment led to a 30% decrease in polarization. Aifm2 KD BAT cells showed a 25% increase in polarization than control cells and Aifm2 KD cells had no decrease in polarization by ISO treatment (Fig. 4A, left). Conversely, Aifm2 OE an approximately 25% decrease in polarization and ISO further decreased polarization by another 25% (Fig. 4A, right). We also utilized TMRM (tertramethylrhodamine) to examine mitochondrial potential. TMRM can also accumulate in polarized mitochondria but disappears in depolarized mitochondria. In Aifm2 KD BAT cells, TMRM positive cell population was 20% higher than control cells. When treated with ISO, TMRM positive control cells decreased by 30%, while no change was detected in Aifm2 KD cells (Fig. S3C). Together, these results indicate Aifm2 increases mitochondria membrane potential.

Next, we measured (OCR) in Aifm2 KD or OE BAT cells by Seahorse XF24. In scrambled shRNA BAT cells, overall OCR increased significantly upon ISO treatment. OCR under oligomycin treatment, which reflects uncoupled respiration, was also increased by approximately 30% upon β-AR stimulation. Notably, Aifm2 KD reduced overall OCR and uncoupled OCR by approximately 30%. Furthermore, Aifm2 KD cells did not show any increase in uncoupled OCR by ISO treatment (Fig. 4B, left). Conversely, in BAT cells OE Aifm2, overall OCR was significantly higher than control cells and uncoupled OCR increased further by 40% (Fig. 4B, right). These findings clearly show that Aifm2 promotes mitochondrial oxidative metabolism and ETC activity in BAT cells. In order to test whether mitochondria association of Aifm2 is critical for its function, Aifm2 G2A mutant, that is mainly found in mitochondria and Aifm2 Δ N, that is not associated with mitochondria were overexpressed in BAT cells. Our data showed that Aifm2ΔN OE cells had lower NAD/NADH level, ECAR and OCR than to Aifm2 WT. In contrast, Aifm2 G2A mutant had increased NAD/NADH ratio, ECAR and OCR compared to Aifm2 WT even in basal condition. This indicates that Aifm2 association with mitochondria increases ETC activity (Fig. S3D).

Next, to determine Aifm2 effect on thermogenesis, we utilized a small molecule thermosensitive fluorescent dye, ERthermAC, which can directly monitor temperature changes in live cells (Kriszt et al., 2017). ERthermAC accumulates in the ER and decreases fluorescence to correspond to an increase in temperature. As expected, there was a large shift in BAT cell distribution to a higher temperature range upon CL-316,248. The average

fluorescence intensity of ERthermAC upon β-agonist decreased by approximately 65%, indicating an increase in cell population at a higher temperature. More importantly, Aifm2 OE increased the cell population of higher temperature by 3-fold, and further increased by 2-fold upon β-agonist (Fig. 4C). Altogether, Aifm2 induced higher OCR, uncoupled respiration and heat production, clearly demonstrate promotion of thermogenesis by Aifm2.

To determine whether Aifm2 function in glycolysis is required for its enhancement of thermogenesis, we tested the effect of Aifm2 on uncoupled OCR in the presence of hexokinase inhibitor, 2-DG (2-deoxyglucose), which effectively blocks glycolysis. With ISO, Aifm2 OE BAT cells had approximately 40% higher overall and uncoupled OCR than control cells. However, the increase in overall and uncoupled OCR by Aifm2 was completely abolished when cells were pre-treated with 2-DG (Fig. 4D, left). Utilizing ERthermAC, as expected, Aifm2 OE BAT cells had a 50% increase in cell population at a higher temperature range compared to the control cells by β-agonist. Remarkably, there was no increase in numbers of cells at higher temperature range in Aifm2 OE BAT cells that were pre-treated with 2-DG (Fig. 4D, right). These results confirm that Aifm2 increases overall mitochondrial activity and promotes thermogenesis in BAT cells by maintaining cytosolic NAD to sustain robust glycolysis.

NADH oxidase activity of Aifm2 is required to sustain glycolysis for thermogenesis

We found Aifm2 increases NAD/NADH to promote glycolysis and ultimately thermogenesis in BAT cells. To test whether NADH oxidase activity of Aifm2 is required for its effects on glycolysis and thermogenesis, we next performed site-directed mutagenesis of D285N at the putative NADH-binding site of Aifm2. The WT and D285N mutant of Aifm2 were overexpressed in BAT cells (Fig. 5A). Unlike AIFM2 WT, D285N mutant showed no NADH oxidase activity in vitro (Fig. 5B, left). Notably, Aifm2 D285N mutant failed to increase NAD/NADH ratio, whereas WT Aifm2 increased NAD/NADH 1.8 and 3.0 -fold in basal and ISO condition, respectively (Fig. 5B, right). While Aifm2 WT OE increased the maximal glycolytic capacity measured by ECAR by approximately 40%, the Aifm2 D285N did not affect glycolysis (Fig. 5C). Additionally, Aifm2 D285N did not enhance overall or uncoupled OCR in BAT cells (Fig. 5D). These results show that NADH oxidase is required for Aifm2 effect on glycolysis and thermogenesis.

We next performed rescue experiments. Aifm2 KO BAT cells were generated by CRISPR-Cas9. A gRNA targeting exon 5 of Aifm2 was introduced by lentivirus into BAT preadipocytes, stably expressing Cas9. We transfected WT and D285N Aifm2 into Aifm2-KO cells. Since Aifm2 have relatively high sequence similarity at 42% with yeast NDE1, an external NADH oxidase, we also used NDE1 for rescue experiments. Overexpression of WT Aifm2, Aifm2 D825N and NDE1 were detected by immunoblotting (Fig. 5E). As expected, Aifm2 KO cells had 40% lower of NAD/NADH than control cells. Cells expressing Aifm2 WT and NDE1 showed an increase in NAD/NADH ratio, whereas Aifm2 D285N mutant failed to do so (Fig. 5F). Moreover, Aifm2 KO had 2-fold lower glycolytic capacity by ECAR. Aifm2 WT and NDE1 OE both increased the glycolytic rate in these Aifm2 KO cells, while Aifm2 D285N failed to rescue glycolysis(Fig. 5G, left). Similarly, lactate level in Aifm2 KO cells was 5-fold lower than WT cells. Both Aifm2 WT and yeast NDE1 OE

increased intracellular lactate level to that in control cells, whereas Aifm2 D285N did not, demonstrating that the NADH oxidase activity of Aifm2 is critical for its function in glycolysis (Fig. 5G, right). Furthermore, overall and uncoupled OCR of Aifm2 KO cells, which was 3-fold lower than control cells, was restored by overexpression of either WT Aifm2 or NDE1, but not Aifm2 D285N (Fig. 5H). Together, these results demonstrate that NADH oxidase activity of Aifm2 is critical for its function in sustaining glycolysis to support thermogenesis and Aifm2, once translocated to mitochondria, can function similar to yeast NDE1.

Aifm2 is critical for thermogenesis *in vivo* in mice

We next tested the role of Aifm2 on thermogenesis *in vivo.* Because Aifm2 is highly expressed only in BAT and not in any other tissues, first, we generated global Aifm2-KO mice, using CRISPR-Cas9 system (Fig. 6A, left). *In vitro* transcribed gRNA and Cas9 mRNA were then injected into zygotes. We verified 3 KO lines by sequencing, including a single nucleotide addition, a 2 bp deletion, a 22 bp deletion in the coding region of the third exon. All lines were confirmed to have complete ablation of Aifm2, and they showed similar phenotypes. Here, the findings from 22 bp deletion KO line were presented. By immunoblotting, Aifm2 was not detectable in BAT or iWAT of Aifm2 KO mice (Fig. 6A, right). The Aifm2 KO mice had higher body weights with increased WAT as determined by EcoMRI (Fig. 6B) and by weighing of dissected WAT depots (Fig. S4A). There was no difference in food intake collected during CLAMS study (Fig. S4B). Histological analysis of whole mount staining of WAT with LipidTox (red) revealed a larger size distribution of Aifm2 KO mice than WT mice. The differences in brown adipocyte size were more apparent in H&E staining (Fig. S4C). The Aifm2-KO mice had greatly reduced expression of BAT-enriched genes, such as UCP1 and Dio2, but interestingly higher expression of adipogenic genes, such as C/EBPβ, C/EBPδ and PPARγ (Fig. S4D). To ensure Aifm2 does not affect brown adipogenesis, Aifm2 was overexpressed in BAT preadipocytes, which was then subjected to differentiation. By RT-qPCR, there was no difference in adipogenic markers, such as C/EBPβ, C/EBPδ and PPARγ, FABP4 as well as thermogenic genes such as UCP1, Dio2 (Fig. S5A–B). In addition, lipid accumulation showed no change in Aifm2 OE BAT cells comparing to the control cells (Fig. S5C). These results suggest that Aifm2 KO had higher adiposity due to defective thermogenic program. Thus, the KO mice could not maintain body temperature upon cold. The average body temperature of KO mice after 5 hrs of cold exposure was 8^{o}C lower than that of WT mice (Fig. 6C, left). Infrared camera was used to document the heat production by BAT. The BAT temperature of KO mice was approximately 6^{o}C lower than that of WT mice (Fig. 6C, middle). After 8 hrs of chronic cold exposure, only 50% of Aifm2 KO mice survived, whereas all WT mice were alive (Fig. 6C, right). Moreover, the whole-body OCR of Aifm2 KO compared to WT littermates measured by CLAMS was significantly lower during the night when mice were kept at 30^{o}C, and both during day and night when mice were kept at 23°C. This decrease in OCR in Aifm2 KO mice was even more apparent at 4°C (Fig. 6D, left). OCR in BAT excised from these mice were 15% lower than one of WT by Seahorse XF-24 (Fig. 6D, right). In addition, both BAT and iWAT of Aifm2 KO had significantly lower NAD/NADH ratio (Fig 6E, left). Intracellular lactate levels in BAT of Aifm2 KO mice were 2-fold lower also (Fig 6E, right). These results indicate that Aifm2 KO had lower glycolytic capacity of BAT. We also

employed Metabolic Flux Analysis using [U-^{13}C]-glucose. Mice fasted for 4 hrs were injected intraperitoneally with [U-^{13}C]-glucose. BAT collected after 1 hr were methanol extracted for metabolite analysis. The isotopomer levels of metabolites were shown as molar fractions, where M+1, M+2, M+3, etc. represent the number of ^{13}C atoms, while M+0 represent endogenous unlabeled metabolites. These results showed effective ^{13}C incorporation into fructose 1,6-bisphosphate (F1,6BP) (M+6), pyruvate(M+3), lactate(M+3) being the predominant isotopomers. More importantly, these metabolites were 2-fold lower in BAT of Aifm2 KO than WT mice. Additionally, TCA cycles metabolites, such as α-ketoglutarate (M+2), fumarate (M+2), malate (M+2), succinate (M+2), citrate(M+2, M+3, M+5), mainly were detected from [U-^{13}C]-glucose] through pyruvate carboxylase (PC) or pyruvate dehydrogenase (PDH) reactions and they were all significant lower in Aifm2 KO compared to WT mice (Fig. 6F, S4E). These results clearly demonstrate Aifm2 depletion decreased glycolysis in BAT. Overall, we conclude that Aifm2 ablation in mice decreases thermogenesis and energy expenditure, resulting in higher adiposity.

To test effect of Aifm2 ablation specifically in BAT and iWAT on thermogenesis, Aifm2 pooled shRNA were injected directly to BAT and iWAT of WT mice via AAV7/9 viruses that are reported to restrict expression in adipose tissue (Jimenez et al., 2013). AAV7/9 viruses carrying scrambled shRNA were used as controls. BAT and iWAT of these mice were evaluated after 2 wks. RT-qPCR showed Aifm2 mRNA levels were 3-fold lower in both BAT and iWAT of Aifm2 shRNA injected mice, while there were no significant differences in pWAT or other tissues. Aifm2 protein levels were lower also by Aifm2 shRNA injection (Fig. S4G). In addition, there was no significant changes in adipogenic markers such as PPARγ C/EBPβ, FABP4 (Fig. S4I). When Aifm2 shRNA AAV7/9 injected mice were subjected to 4°C for 4 hrs, average body temperature was 3°C lower than control mice (Fig. S4H, left). Moreover, whole-body OCR of Aifm2 shRNA injected mice was significantly lower than the control mice at RT, and was even more significant at 4°C (Fig. 4H, right). We also employed lentivirus for Aifm2 shRNA directly to BAT and iWAT of WT mice. After 2-wks, Aifm2 mRNA levels to be 2-fold lower in both BAT and iWAT of Aifm2 shRNA lentivirus injected mice than control shRNA injected mice (Fig. S4J). Similar to Aifm2 AAV-shRNA injected mice, these mice have lower rectal temperature and BAT, accompanied with lower whole-body OCR with no difference in adipogenic and thermogenic markers (Fig. S4K–L). These results indicate Aifm2 effect is due to its function in glycolysis, but not adipocyte differentiation.

To further determine the role of Aifm2 specifically in BAT *in vivo,* we generated Aifm2 floxed mice using CRISPR-Cas9 Nickase system (Fig. 6J, left). To generate BAT specific KO of Aifm2 (Aifm2 BKO), we injected homozygous Aifm2 floxed mice with UCP1-Cre AAV7 virus that we constructed by inserting Cre into 3' end of the −2.8 kb UCP1 promoter to express Cre in UCP1^{+} cells in adults (Kozak et al., 1994). Control mice were floxed mice that were injected AVV control virus. Along with the pair of gRNAs, *in vitro* transcribed gRNA and Cas9 Nickase mRNA were injected into zygotes. RT-qPCR showed Aifm2 mRNA to be reduced by 10-fold and 5-fold in BAT and iWAT, respectively, while there was no difference in pWAT, kidney, and muscles (Fig. S4M). Immunoblotting also showed a significantly lower Aifm2 protein levels in Aifm2-BKO mice (Fig. 6H). When subjecting to 4°C, Aifm2-BKO mice had 4°C lower body temperature than Aifm2 floxed mice. Moreover,

whole-body OCR of Aifm2-BKO mice was lower at all temperatures than the floxed mice, the difference being more significant at both 23°C and 4°C than at 30°C (Fig. 6I). When BAT depots were and subjected to Seahorse, whole-body OCR in BAT of Aifm2 BKO was approximately 33% lower than one in WT mice (Fig. S4N). Taken together, these results show that Aifm2 ablation specifically in UCP1$^+$ cells in vivo results in decreased OCR and impaired thermogenesis.

Next, we generated transgenic mice overexpressing Aifm2 in UCP1$^+$ cells for conditional gain-of function studies. We constructed a plasmid in which the chicken β-actin promoter driving the Aifm2 tagged with zsGreen and the bovine growth hormone poly A signal at the 3' end. We inserted LoxP-STOP-LoxP casette at the 5' of the Aifm2 coding sequence to allow Cremediated conditional excison of stop codon for Aifm2 expression (Fig. 6J, top). And these mice were crossed with UCP1-Cre mice to overexpress Aifm2 only in UCP1$^+$ cells. RT-qPCR and immunoblotting of Aifm2 showed overexpression in both BAT and iWAT of Aifm2 TG mice (Fig. 6J, bottom and S6A). Body weight and EcoMRI scanning showed that these mice had lower body weight with smaller WAT mass without any differences in lean mass than WT mice (Fig. 6K). It is confirmed by dissecting and weighing of each WAT depots (Fig. S6B). H&E staining revealed not much difference in morphology of BAT between Aifm2 TG and WT (Fig. S6C). There was no difference in food intake (Fig. S6D). The TG mice had higher levels of BAT and thermogenic genes, such as UCP1, Dio2 and Cidea, but had lower adipogenic markers, such as Sox9 (Fig. S6E). Aifm2 TG mice could maintain body temperature better when exposed at 4°C. After 5 hrs at 4°C, body temperature of Aifm2-TG mice was decreased only by 1°C, while that of WT littermates dropped by 4°C (Fig. 6L, left). After 12 hrs at cold, BAT of Aifm2 TG mice showed higher temperature, by 8°C compared to WT mice as detected by the infrared camera (Fig. 6L, right). Moreover, 80% of Aifm2-TG mice survived, whereas only 20% WT mice remained after longer cold exposure (Fig. S6F). The Aifm2-TG mice showed a higher wholebody OCR at 30°C during night, and 23°C during both day and night than WT littermates, and the increase in OCR was even more significant at 4°C (Fig. 6M). OCR of BAT and iWAT of Aifm2 TG mice by Seahorse was also higher than that of WT littermates (Fig. 6N). Moreover, the NAD/NADH ratio was 2-fold higher in iWAT and BAT of Aifm2 TG mice than WT littermates (Fig. 6O, left). BAT of Aifm2 TG showed 2-fold higher lactate levels than BAT of WT (Fig. 6O, right). The Aifm2-TG mice had a greater thermogenic capacity and energy expenditure, which led to lower adiposity and leaner phenotype. Overall, these results of loss- and gain-of-function in vivo clearly demonstrate evidence for the critical role of Aifm2 in thermogenesis in BAT and that Aifm2 increases glycolysis and OCR to enhance thermogenesis resulting in decreased adiposity in mice.

Aifm2 promotes glucose oxidation for cold- and diet-induced thermogenesis

In contrast to the fasted state in which BAT may primarily use FFA released from WAT lipolysis for thermogenesis, BAT may use glucose for oxidation in the fed state to fuel thermogenesis. We next tested if Aifm2 functions in response to diet or fed state when glucose is abundant. We evaluated substrate preference in fueling thermogenesis in BAT cells. We compared V_{CO2}/V_{O2} from the OCR by Seahorse. V_{CO2}/V_{O2} in basal condition was 0.87 and 0.81 in control and Aifm2 KD BAT cells, respectively, showing that Aifm2

depletion shifted the ratio somewhat toward FA oxidation. Remarkably, when treated with ISO, the V_{CO2}/V_{O2} ratio in control BAT cells increased to 0.95, whereas the ratio in Aifm2 KD cells failed to increase (Fig. 7A, left). Conversely, Aifm2 OE shifted V_{CO2}/V_{O2} ratio from 0.87 to 0.90, a slight shift toward glucose oxidation in the basal condition. Notably, ISO treatment of Aifm2 OE cells further shifted V_{CO2}/V_{O2} to 1.00, an indication of exclusive glucose utilization (Fig. 7A, right). Similar to BAT cells in culture, Aifm2 KO mice showed a lower whole-body V_{CO2}/V_{O2} of 0.76 compared to the WT of 0.84, whereas Aifm2 TG mice had V_{CO2}/V_{O2} of 0.9. Aifm2 BKO also had lower whole-body V_{CO2}/V_{O2} of 0.77 than 0.82 of Aifm2 floxed control mice (Fig. 7E). Overall, these data establish that Aifm2 not only increases glycolysis but promotes further oxidation of glucose of BAT during thermogenesis.

To examine whether Aifm2 effect on thermogenesis is due to glucose oxidation, Aifm2 OE BAT cells were treated with UK5009, an inhibitor of mitochondrial pyruvate carrier (MPC), to prevent pyruvate transport into mitochondria. MCP inhibition was reported to block lactate uptake due to accumulation of intracellular pyruvate. With the β-AR stimulation, Aifm2 OE BAT cells showed a 40% increase in uncoupled OCR, and this increase was lost with the MCP inhibitor treatment. MCP inhibitor also decreased uncoupled OCR in the control cells, indicating glucose oxidation for thermogenesis and Aifm2 effect on thermogenesis as well (Fig. 7B). In contrary, when Aifm2 OE BAT cells were treated with carnitine palmitoyltransferase 1 (CPT1) inhibitor, Etomoxir, to prevent FA transport into mitochondria, Aifm2 still increased overall and uncoupled OCR (Fig. 7C). Next, we measured OCR in BAT cells maintained in media containing either glucose or FA only. Similar to that observed in cells in complete media, OCR was higher in Aifm2 OE cells compared to control cells in glucose only containing media. But this increase in OCR was not detected when cells were maintained in palmitate only media (Fig. 7D, left). We next measured the heat production to test the effect of Aifm2 on thermogenesis in BAT cells maintained in glucose or FA only. Indeed, Aifm2 OE BAT cells had higher heat production by ERthermAC than control cells in the presence of glucose only, but not in the presence of palmitate only (Fig. 7D, right). These results support the notion that BAT cells can utilize glucose to fuel thermogenesis and that Aifm2 effect on thermogenesis is dependent on its function in glycolysis and glucose oxidation.

Our results so far showed Aifm2 can sustain glycolysis and glucose utilization to support thermogenesis during cold exposure. Next, we wanted to investigate whether Aifm2 functions in diet-induced thermogenesis. Thus, we compared Aifm2 expression in fasted and fed condition. Mice kept at 30ºC were either fasted or given a high carbohydrate diet (HCD) overnight. Indeed, similar to UCP1, Aifm2 mRNA increased by 2- and 4-fold in BAT and iWAT, respectively, in HCD mice. Immunoblotting revealed a similar increase in Aifm2 protein levels (Fig. 7F). WT and Aifm2 TG mice were then fasted at 30ºC for 6 hrs and half of each group was given HCD. OCR was measured for 20 hrs by CLAMS. Some activity was observed early in HCD treated mice due their immediately consumption of food at right after a period of fasting. The data showed that fasted Aifm2 TG mice on HCD had lower whole-body OCR than WT. More importantly, Aifm2 TG mice had significant higher OCR than WT mice only in the HCD fed state but failed to maintain the level in the fasted state (Fig. 7G), indicating that Aifm2 effects on OCR requires glucose. Overall, by increasing

NAD levels to support robust glycolysis, Aifm2 is critical, not only for cold-induced, but also for diet-induced thermogenesis.

DISCUSSION

Aifm2, a FAD dependent NADH/NAD oxidoreductase, belongs to Apoptosis Inducing Factor (AIF) family of proteins, having 22% identity and 44% similarity with AIF. While AIF was reported to be widely expressed in various organs, Aifm2 is very low in many tissues but expressed at a high level mainly in BAT and that Aifm2 in BAT is induced by cold exposure and by diet. Moreover, upon cold-exposure, Aifm2 is induced in subcutaneous WAT, a WAT depot that undergoes beiging. With its NADH oxidase activity, we show that Aifm2 maintains a robust glycolytic rate by generating NAD in cytosol to promote thermogenesis.

It has recently been reported that FFAs released from WAT, rather than those from intracellular lipolysis, are utilized for thermogenesis in BAT, particularly in the fasted state (Shin et al., 2017, Schreiber et al., 2017). Our studies demonstrate BAT utilizes glucose via glycolysis upon cold, especially in the fed state, and that Aifm2 is required for optimal glycolysis. In this regard, glucose utilization in BAT was reported to be diminished in UCP1 KO mice treated with norepinephrine (Inokuma et al., 2005). Remarkably, Aifm2 expression is induced not only by cold but also by diet even at thermoneutrality. Not much is known about the function of Aifm2 in BAT. Aifm2 has been reported to be a p53 target and a tumor suppressor by inducing apoptosis (Mei et al., 2006, Wu et al., 2004). However, the Aifm2 KO mouse model reported previously did not develop tumor, nor the authors noted any phenotypes related to obesity or thermogenesis (Mei et al., 2006). We found Aifm2 overexpression in BAT cells did not induce apoptosis (Fig. S2). Possibly, we propose that Aifm2 may even promote tumor growth by enhancing aerobic glycolysis.

Some studies have proposed that glucose is an energy source to fuel thermogenesis, particularly in postprandial thermogenesis, with an increase in insulin secretion (M et al., 2018). However, the fate of glucose metabolism after glycolysis was not clear. Pyruvate produced from glycolysis may be transported into mitochondria to be oxidized via TCA cycle. Moreover, citrate from TCA cycle is transported to cytoplasm for de novo lipogenesis, which can explain how lipogenesis and lipolysis may increase in parallel during thermogenesis (Yu et al., 2002, Barquissau et al., 2016). Pyruvate may also be used for anaplerosis to replenish TCA cycle intermediates (Cannon and Nedergaard, 1979) that might even be required for FA oxidation (Winther et al., 2018). In our study, we show glycolysis increase significantly upon β-AR stimulation and blocking glycolysis and glucose oxidation decreased OCR and heat production even in the presence of FAs. This notion is supported by our observation that mice that are fasted have lower OCR and body temperature compared to fed mice (Data not shown). The effect of Aifm2 on thermogenesis in BAT cells is completely dependent on glucose oxidation since blocking glucose oxidation by inhibiting pyruvate transport into mitochondria diminishes thermogenesis increased by Aifm2 overexpression. These findings demonstrate that Aifm2 is essential for robust glycolysis and subsequent glucose oxidation to maximize thermogenic capacity.

In order to maintain robust glycolysis during thermogenesis, high cytosolic NAD level is essential for BAT. Interestingly, we found that Aifm2 can translocate to mitochondrial inner membrane facing the interspace and, upon cold exposure or β-AR stimulation, NAD is generated by its NADH oxidase activity. Aifm2 isolated from either LD or mitochondrial fraction of BAT cells showed similar Km and Vmax for NADH oxidase activity (Fig. S7). We propose that Aifm2 translocated from LD to mitochondria, not only to increase cytosolic NAD, but also to support ETC. At this time, the mode of regulation that explains how cold exposure /β-AR stimulation can increase Aifm2 association with mitochondria is not known. In order to explore the regulation of Aifm2 translocation to mitochondria during thermogenesis, we tested Nmyristoylation of Aifm2 under β-AR stimulation. However, there was no changes of Nmyristoylation of Aifm2 during thermogenesis, indicating that myristoylation is not critical for Aifm2 translocation to mitochondria (Fig S3E). Next, we measured ex vivo lipolysis. Although no significant difference in lipolysis between Aifm2 KO and WT mice, as expected, lipolysis was increased in the stimulated compared to basal condition in WT and KO mice (Fig. S4F). It is possible that as lipolysis increases during thermogenesis, LDs get smaller and Aifm2 might translocate from LD to mitochondria due to lacking binding surface. Thus, it should be further explored in the future.

Although mtGPD has been presumed to regenerate cytosolic NAD level in BAT, the role of mtGPD in glycolysis remains unclear, since its importance in thermogenesis could not be demonstrated in mtGPD knockout mouse models (Alfadda et al., 2004). We propose that Aifm2 represents a unique BAT specific mechanism for NAD regeneration to sustain high glycolytic flux during thermogenesis by its NADH oxidase enzymatic activity. Interestingly, Aifm2 shares sequence similarity to yeast NDE1, a NADH oxidoreductase that associates with the mitochondrial inner membrane and faces the mitochondrial intermembrane space and maintains cytosolic NAD to support glycolysis (Luttik et al., 1998b). We propose that Aifm2 acts as a mammalian NDE by associating with the mitochondrial inner membrane. With the same enzymatic activity and localization, we argue that Aifm2 is a mammalian NDE specifically present in thermogenic tissues.

The phenotype of our loss- and gain-of function mouse models firmly establish the physiological significance of Aifm2 in thermogenesis; Aifm2 total and BAT specific deficiency in mice significantly impairs glycolytic capacity, thermogenesis and cold tolerance which led to decreased energy expenditure and higher adiposity. Conversely, Aifm2 overexpression in BAT enhances thermogenesis, protecting mice from diet induced obesity. Although mitochondrial Complex I is present in BAT, Aifm2 as a mammalian NDE, can maximize glycolysis and glucose oxidation and provide elections to ETC to fuel UCP1 for thermogenesis by associating with the mitochondrial inner membrane.

STAR Methods

LEAD CONTACT AND MATERIALS AVAILABILITY

Further information and requests for resoucres and reagents should be directed to and will be fulfilled by the Lead Contact, Hei Sook Sul (hsul@berkeley.edu). All plasmids generated in this study will be made available on request but we may require a payment and/or a completed Materials Transfer Agreement if there is potential for commercial application.

EXPERIMENTAL MODEL AND SUBJECT DETAILS

All animal studies were carried out in accordance with UC Berkeley ACUC and OLAC regulations. Generation of Aifm2 KO mice was created by injecting Cas9 mRNA and an in vitro transcribed guide RNA target sequence, CTTCCCTGGCAAGTTTAACG, corresponding to aa113–120 at the third exon of Aifm2 into zygotes. Aifm2 was first inserted into plasmid in which the chicken β-actin promoter driving tagged zsGreen and the bovine growth hormone poly A signal at the 3' end. The vector also contains LoxP-STOP-LoxP cassette at 5' end of the Aifm2 coding sequence. Generation of Aifm2 floxed mice was carried out by microinjected into embryos. Aifm2 TG mice were generated by crossing these mice with UCP1-Cre mice. Aifm2 floxed mice using CRISPR-Cas9 Nickase system. A pair of the gRNAs target sequences, ACCAGCGGCTCGAGCCTCTCAGG and GTAAATCTCAGGACAGCGCTAGG, corresponding to 5' and 3' end of Exon 2 of the Aifm2 gene, respectively, with Cas9 Nickase mRNA, and DNA donor containing Exon2 flanked by LoxP sites were injected into zygotes. Mice were housed in a 12:12 light-dark cycle and chow and water were provided *ad libitum,* when not specified.

Metabolic and thermogenic measurements—Fat and lean mass was determined by echoMRI-100V. CT Scan was performed on Trifoil eXplore RS9 microCT system. Oxygen consumption was measured using the Comprehensive Laboratory Animal Monitoring System (CLAMS). Data were normalized to lean body mass determined by EchoMRI. Mice were individually caged and maintained under a 12 hr light/12 hr dark cycle. Food consumption and locomotor activity were tracked. Cold exposed mice were housed for 10 days at thermoneutrality before cold exposure at 4°C. Body temperatures were assessed using a RET-3 rectal probe for mice (Physitemp). CL316,243 (Sigma) was intraperitoneally injected into mice at 1mg/kg. FLIR E5 series infrared camera was employed to capture thermography.

Human tissues—Human cDNA array containing cDNA from 48 samples covering all major human normal tissues at different locations (Origene, HRMT104) were used for RT-qPCR and human tissue lysates (Thermo) were utilized immunoblotting.

Cell culture—Brown adipocyte differentiation was performed as described in (Kajimura et al., 2008). To induce thermogenic genes, cells were treated for 6 hrs with 10 μM isoproterenol or CL316,248. Cells were then harvested for RNA isolation or protein extraction or fixed with formalin for ORO staining. For adenoviral transduction, sub-confluent BAT cells were transduced with vehicle (ViraQuest) or Aifm2 (Abmgood) lentivirus with 0.5 μg/ml polyLysine at MOI=100. For Aifm2 knockdown, BAT adipocytes were transduced by Aifm2 shRNA lentivirus at MOI=200.

Whole mount staining—1mm piece of tissue was excised, fixed with 1% PFA, incubated with UCP1 antibody, LipidTox Red Reagent (Thermo Fisher) and DAPI. Tissues were immobilized on a slide with mounting medium and visualized using a confocal microscope.

Mitochondria and lipidTox analysis—MitoTracker Red was added into the culture media at final concentrations of 300nM. The cells were incubated under normal culture

conditions for 15 min. LipidTox Red was added into the culture media at 1:200 dilution. The cells were incubated under normal culture conditions for 30 min. These cells were mounted with Duolink Mounting medium with DAPI, and then visualized by fluorescence microscopy.

Plasmid Constructs—Aim2 N-terminal and C-terminal deletion constructs were created by PCR amplifying the non-deleted part of the vector and reinserting into either pCDNA3.1 or pEGFP-C1. Aifm2 D285N and G2A mutants were created by site directed mutagenesis using the following primers indicated in Table S1.

Luciferase Assays—293FT cells were transfected with 300ng CREB or empty vector with 100 ng of indicated Aifm2 promoter luciferase reporter construct and 0.5ng pRL-CMV in 24-well plates with Lipofectamin2000 reagent. Cells were lysed 48h post-transfection and assayed for luciferase activity using the Dual-Luciferase Kit (Promega) according to manufacturer recommended protocol.

Separation of SVF and Adipocyte fraction—SVF fractionation was carried out as previously described[12]. Briefly, mouse WAT and BAT were minced and digested with Collagenase type II (Sigma) in KREBs buffer at 37° C for 45 min with shaking. Cell suspension was then passed through 100 μm mesh, span at 300g for 5 min, floating adipocyte fraction was collected for RNA, DNA, or protein extraction, whereas cell pellet was resuspended in KREBS buffer, passed through 70 μm and 40 μm mesh and subjected to FACS and *in vitro* differentiation, or lysed with RIPA buffer for immunoblotting or with TRIzol for RNA isolation.

RNA isolation and RT-qPCR—Total RNA from cells were extracted using TRIzol and RNA from adipose tissue were extracted using RNeasy Lipid kit (Qiagen). Reverse transcription was performed with 1 μg of total RNA using Superscript II (Invitrogen) or with 10–100 ng from sorted cells using Superscript III (Invitrogen). RT-qPCR was performed on ABI PRISM 7500 (Applied Biosystems). Statistical analysis was performed using ddct method with U36B4 primers as control (see primer sequences in Supplementary Table S1.

Whole mount staining—1mm piece of tissue was excised, fixed with 1% PFA, incubated with UCP1 antibody, LipidTox Red Reagent (Thermo Fisher) and DAPI. Tissues were immobilized on a slide with mounting medium and visualized using a confocal microscope.

Immunoblotting and Immunostaining—For immunoblotting, tissues or cells were lysed in RIPA buffer. Proteins (5–100 μg) were separated on SDS-PAGE gel, transferred on a nitrocellulose membrane and incubated with indicated antibodies. For whole-mount tissue immunostaining, a 1mm piece of WAT or BAT was excised, incubated with LipidTOX Reagent (Thermo Fisher) and DAPI, immobilized on a slide with mounting medium and imaged using confocal microscope. Cell number and size was calculated using ImageJ software.

Seahorse assay—BAT cell line cells were differentiated in 12-well plates, trysinized, and reseeded in XF24 plates at 50K cells per well at day 4 of differentiation and assayed on day

5 of differentiation. On the day of experiments, the cells were washed three times and maintained in XF-DMEM (SigmaAldrich) supplemented with 1 mM sodium pyruvate and 17.5 mM glucose. Oxygen consumption was blocked by 1 μM oligomycin. Maximal respiratory capacity was assayed by the addition of 1 μM FCCP. Tissues were incubated for 1 hour at 37°C w ithout CO_2 prior to analysis on the XF24 Analyzer.

AAV and lentivirus administration in animals—Mice were anesthetized with ketamine (100 mg/kg). For administration into BAT and WAT, a longitudinal incision in the skin at the interscapular or inguinal area was performed. To distribute the vector in the whole depot, each interscapular BAT (iBAT) or inguinal WAT (iWAT) received four injections of 20 μL AAV or Aifm2 shRNA solution using a Hamilton syringe. For the systemic administration, AAV vectors were diluted in 200 μL saline and injected into the lateral tail vein.

Subcellular fractionation—Mitochondrial fractions were isolated with 50 mg of brown adipose tissue or 2×10^7 using Mitochondria Isolation Kit for Tissue or Culture Cells (Thermo Scientific). LD and cytosolic fractions were isolated as described in (Harris et al., 2012).

Mitochondria and mitoplast isolation—Intact mitochondria from adipose tissues or BAT cells were isolated using Mitochondria Isolation Kit. Mitochondrial extract was collected using 2% CHAPS lysis buffer. Intact mitoplast preparation was isolated by treating purified mitochondria with digitonin (0.25mg/ml) for 20 min.

NAD/NADH and NADH oxidase activity—NAD/NADH in cell/ tissue lysates was measured with colorimetric NAD/NADH (K337). Oxidoreductase activity assay was carried out by using spectrophotometer, as described in Miramar et al, 2001. The assay buffer contained 100 mM potassium phosphate pH, 8.0, 100 mM NaCl and 0.1 mM FAD. Enzyme was mixed in the assay buffer for 15 min prior to adding NADH to final concentration of 0.25 mM. The absorbance at 340 nm was measuring at 25^{o}C.

JC-1 and ERthermAC—BAT cells ($1X10^6$ cells/ml) were treated with JC-1 (2 μM) for 30 min, and cells were then washed 2 times with PBS and subjected to FACS analysis. For ERthermAC, BAT cells were treated with the dye (250 nM) for 30 min prior to FACS analysis.

Statistical analysis—Statistical analysis was performed using two tailed t-test. The error bars represent standard deviation (SD). Data are expressed as mean +/− SD and p value <0.05 was considered statistically significant. Number of mice or replicates used in each experiment was indicated in figure legends. Experiments were repeated at least three times.

Data availability statement—The data that support the findings of this study are available from the corresponding author H.S.S. upon request.

Supplementary Material

Refer to Web version on PubMed Central for supplementary material.

ACKNOWLEDGEMENTS

The work was supported in part by NIDDK-R01DK112824 grant to H.S.S. Imaging was supported in part by NIH S10RR026866-01. The content is solely the responsibility of the authors and does not necessarily represent the official views of the NIH. The authors declare no competing financial interests.

REFERENCES

Bartelt A & Heeren J 2014 Adipose tissue browning and metabolic health. Nat Rev Endocrinol, 10, 24–36. [PubMed: 24146030]

Cypess AM, Lehman S, Williams G, Tal I, Rodman D, Goldfine AB, Kuo FC, Palmer EL, Tseng YH, Doria A, Kolodny GM & Kahn CR 2009 Identification and importance of brown adipose tissue in adult humans. N Engl J Med, 360, 1509–17. [PubMed: 19357406]

Virtanen KA, Lidell ME, Orava J, Heglind M, Westergren R, Niemi T, Taittonen M, Laine J, Savisto NJ, Enerback S & Nuutila P 2009 Functional brown adipose tissue in healthy adults. N Engl J Med, 360, 1518–25. [PubMed: 19357407]

Nedergaard J, Bengtsson T & Cannon B 2010 Three years with adult human brown adipose tissue. Ann N Y Acad Sci, 1212, E20–36. [PubMed: 21375707]

Van Marken Lichtenbelt WD, Vanhommerig JW, Smulders NM, Drossaerts JM, Kemerink GJ, Bouvy ND, Schrauwen P & Teule GJ 2009 Cold-activated brown adipose tissue in healthy men. N Engl J Med, 360, 1500–8. [PubMed: 19357405]

Carpentier AC, Blondin DP, Virtanen KA, Richard D, Haman F & Turcotte EE 2018 Brown Adipose Tissue Energy Metabolism in Humans. Front Endocrinol (Lausanne), 9, 447. [PubMed: 30131768]

Cannon B & Nedergaard J 2004 Brown adipose tissue: function and physiological significance. Physiol Rev, 84, 277–359. [PubMed: 14715917]

Feldmann HM, Golozoubova V, Cannon B & Nedergaard J 2009 UCP1 ablation induces obesity and abolishes diet-induced thermogenesis in mice exempt from thermal stress by living at thermoneutrality. Cell Metab, 9, 203–9. [PubMed: 19187776]

Blondin DP, Frisch F, Phoenix S, Guerin B, Turcotte EE, Haman F, Richard D & Carpentier AC 2017 Inhibition of Intracellular Triglyceride Lipolysis Suppresses Cold-Induced Brown Adipose Tissue Metabolism and Increases Shivering in Humans. Cell Metab, 25, 438–447. [PubMed: 28089568]

Ahmadian M, Abbott MJ, Tang T, Hudak CS, Kim Y, Bruss M, Hellerstein MK, Lee HY, Samuel VT, Shulman GI, Wang Y, Duncan RE, Kang C & Sul HS 2011 Desnutrin/ATGL is regulated by AMPK and is required for a brown adipose phenotype. Cell Metab, 13, 739–48. [PubMed: 21641555]

Schreiber R, Diwoky C, Schoiswohl G, Feiler U, Wongsiriroj N, Abdellatif M, Kolb D, Hoeks J, Kershaw EE, Sedej S, Schrauwen P, Haemmerle G & Zechner R 2017 Cold-Induced Thermogenesis Depends on ATGL-Mediated Lipolysis in Cardiac Muscle, but Not Brown Adipose Tissue. Cell Metab, 26, 753–763 e7. [PubMed: 28988821]

Shin H, Ma Y, Chanturiya T, Cao Q, Wang Y, Kadegowda AKG, Jackson R, Rumore D, Xue B, Shi H, Gavrilova O & Yu L 2017 Lipolysis in Brown Adipocytes Is Not Essential for Cold-Induced Thermogenesis in Mice. Cell Metab, 26, 764–777 e5. [PubMed: 28988822]

M UD, Saari T, Raiko J, Kudomi N, Maurer SF, Lahesmaa M, Fromme T, Amri EZ, Klingenspor M, Solin O, Nuutila P & Virtanen KA 2018 Postprandial Oxidative Metabolism of Human Brown Fat Indicates Thermogenesis. Cell Metab, 28, 207–216 e3. [PubMed: 29909972]

Symonds ME, Aldiss P, Pope M & Budge H 2018 Recent advances in our understanding of brown and beige adipose tissue: the good fat that keeps you healthy. F1000Res, 7.

Winther S, Isidor MS, Basse AL, Skjoldborg N, Cheung A, Quistorff B & Hansen JB 2018 Restricting glycolysis impairs brown adipocyte glucose and oxygen consumption. Am J Physiol Endocrinol Metab, 314, E214–e223. [PubMed: 29118013]

Jeong JH, Chang JS & Jo YH 2018 Intracellular glycolysis in brown adipose tissue is essential for optogenetically induced nonshivering thermogenesis in mice. Sci Rep, 8, 6672. [PubMed: 29704006]

Barron JT, Gu L & Parrillo JE 1998 Malate-aspartate shuttle, cytoplasmic NADH redox potential, and energetics in vascular smooth muscle. J Mol Cell Cardiol, 30, 1571–9. [PubMed: 9737943]

Kauppinen RA, Sihra TS & Nicholls DG 1987 Aminooxyacetic acid inhibits the malateaspartate shuttle in isolated nerve terminals and prevents the mitochondria from utilizing glycolytic substrates. Biochim Biophys Acta, 930, 173–8. [PubMed: 3620514]

Dossantos RA, Alfadda A, Eto K, Kadowaki T & Silva JE 2003 Evidence for a compensated thermogenic defect in transgenic mice lacking the mitochondrial glycerol-3-phosphate dehydrogenase gene. Endocrinology, 144, 5469–79. [PubMed: 12960027]

Alfadda A, Dossantos RA, Stepanyan Z, Marrif H & Silva JE 2004 Mice with deletion of the mitochondrial glycerol-3-phosphate dehydrogenase gene exhibit a thrifty phenotype: effect of gender. Am J Physiol Regul Integr Comp Physiol, 287, R147–56. [PubMed: 15031134]

Vergnes L & Reue K 2014 Adaptive thermogenesis in white adipose tissue: is lactate the new brown(ing)? Diabetes, 63, 3175–3176. [PubMed: 25249643]

Yamashita T, Inaoka DK, Shiba T, Oohashi T, Iwata S, Yagi T, Kosaka H, Miyoshi H, Harada S, Kita K & Hirano K 2018 Ubiquinone binding site of yeast NADH dehydrogenase revealed by structures binding novel competitive- and mixed-type inhibitors. Scientific Reports, 8, 2427. [PubMed: 29402945]

Iwata M, Lee Y, Yamashita T, Yagi T, Iwata S, Cameron AD & Maher MJ 2012 The structure of the yeast NADH dehydrogenase (Ndi1) reveals overlapping binding sites for water- and lipid-soluble substrates. Proc Natl Acad Sci U S A, 109, 15247–52.

Melo AM, Bandeiras TM & Teixeira M 2004 New insights into type II NAD(P)H:quinone oxidoreductases. Microbiol Mol Biol Rev, 68, 603–16. [PubMed: 15590775]

Luttik MA, Overkamp KM, Kotter P, De Vries S, Van Dijken JP & Pronk JT 1998a The Saccharomyces cerevisiae NDE1 and NDE2 genes encode separate mitochondrial NADH dehydrogenases catalyzing the oxidation of cytosolic NADH. J Biol Chem, 273, 24529–34.

Elguindy MM & Nakamaru-Ogiso E 2015 Apoptosis-inducing Factor (AIF) and Its Family Member Protein, AMID, Are Rotenone-sensitive NADH:Ubiquinone Oxidoreductases (NDH-2). J Biol Chem, 290, 20815–26.

Marshall KR, Gong M, Wodke L, Lamb JH, Jones DJ, Farmer PB, Scrutton NS & Munro AW 2005 The human apoptosis-inducing protein AMID is an oxidoreductase with a modified flavin cofactor and DNA binding activity. J Biol Chem, 280, 30735–40.

Ohiro Y, Garkavtsev I, Kobayashi S, Sreekumar KR, Nantz R, Higashikubo BT, Duffy SL, Higashikubo R, Usheva A, Gius D, Kley N & Horikoshi N 2002 A novel p53-inducible apoptogenic gene, PRG3, encodes a homologue of the apoptosis-inducing factor (AIF). FEBS Lett, 524, 163–71. [PubMed: 12135761]

Dupuis J, Langenberg C, Prokopenko I, Saxena R, Soranzo N, Jackson AU, Wheeler E, Glazer NL, Bouatia-Naji N, Gloyn AL, Lindgren CM, Magi R, Morris AP, Randall J, Johnson T, Elliott P, Rybin D, Thorleifsson G, Steinthorsdottir V, Henneman P, Grallert H, Dehghan A, Hottenga JJ, Franklin CS, Navarro P, Song K, Goel A, Perry JR, Egan JM, Lajunen T, Grarup N, Sparso T, Doney A, Voight BF, Stringham HM, Li M, Kanoni S, Shrader P, Cavalcanti-Proenca C, Kumari M, Qi L, Timpson NJ, Gieger C, Zabena C, Rocheleau G, Ingelsson E, An P, O'connell J, Luan J, Elliott A, Mccarroll SA, Payne F, Roccasecca RM, Pattou F, Sethupathy P, Ardlie K, Ariyurek Y, Balkau B, Barter P, Beilby JP, Ben-Shlomo Y, Benediktsson R, Bennett AJ, Bergmann S, Bochud M, Boerwinkle E, Bonnefond A, Bonnycastle LL, Borch-Johnsen K, Bottcher Y, Brunner E, Bumpstead SJ, Charpentier G, Chen YD, Chines P, Clarke R, Coin LJ, Cooper MN, Cornelis M, Crawford G, Crisponi L, Day IN, De Geus EJ, Delplanque J, Dina C, Erdos MR, Fedson AC, Fischer-Rosinsky A, Forouhi NG, Fox CS, Frants R, Franzosi MG, Galan P, Goodarzi MO, Graessler J, Groves CJ, Grundy S, Gwilliam R, Gyllensten U, Hadjadj S, et al. 2010 New genetic loci implicated in fasting glucose homeostasis and their impact on type 2 diabetes risk. Nat Genet, 42, 105–16. [PubMed: 20081858]

Speliotes EK, Willer CJ, Berndt SI, Monda KL, Thorleifsson G, Jackson AU, Lango Allen H, Lindgren CM, Luan J, Magi R, Randall JC, Vedantam S, Winkler TW, Qi L, Workalemahu T, Heid

IM, Steinthorsdottir V, Stringham HM, Weedon MN, Wheeler E, Wood AR, Ferreira T, Weyant RJ, Segre AV, Estrada K, Liang L, Nemesh J, Park JH, Gustafsson S, Kilpelainen TO, Yang J, Bouatia-Naji N, Esko T, Feitosa MF, Kutalik Z, Mangino M, Raychaudhuri S, Scherag A, Smith AV, Welch R, Zhao JH, Aben KK, Absher DM, Amin N, Dixon AL, Fisher E, Glazer NL, Goddard ME, Heard-Costa NL, Hoesel V, Hottenga JJ, Johansson A, Johnson T, Ketkar S, Lamina C, Li S, Moffatt MF, Myers RH, Narisu N, Perry JR, Peters MJ, Preuss M, Ripatti S, Rivadeneira F, Sandholt C, Scott LJ, Timpson NJ, Tyrer JP, Van Wingerden S, Watanabe RM, White CC, Wiklund F, Barlassina C, Chasman DI, Cooper MN, Jansson JO, Lawrence RW, Pellikka N, Prokopenko I, Shi J, Thiering E, Alavere H, Alibrandi MT, Almgren P, Arnold AM, Aspelund T, Atwood LD, Balkau B, Balmforth AJ, Bennett AJ, Ben-Shlomo Y, Bergman RN, Bergmann S, Biebermann H, Blakemore AI, Boes T, Bonnycastle LL, Bornstein SR, Brown MJ, Buchanan TA, et al. 2010 Association analyses of 249,796 individuals reveal 18 new loci associated with body mass index. Nat Genet, 42, 937–48. [PubMed: 20935630]

Heid IM, Jackson AU, Randall JC, Winkler TW, Qi L, Steinthorsdottir V, Thorleifsson G, Zillikens MC, Speliotes EK, Magi R, Workalemahu T, White CC, Bouatia-Naji N, Harris TB, Berndt SI, Ingelsson E, Willer CJ, Weedon MN, Luan J, Vedantam S, Esko T, Kilpelainen TO, Kutalik Z, Li S, Monda KL, Dixo AL., Holmes CC., Kaplan LM., Liang L., Min JL., Moffatt MF., Molony C., Nicholson G., Schadt EE., Zondervan KT., Feitosa MF., Ferreira T., Lango Allen H., Weyant RJ., Wheeler E., Wood AR., Estrada K., Goddard ME., Lettre G., Mangino M., Nyholt DR., Purcell S., Smith AV., Visscher PM., Yang J., Mccarroll SA., Nemesh J., Voight BF., Absher D., Amin N., Aspelund T., Coin L., Glazer NL., Hayward C., Heard-Costa NL., Hottenga JJ., Johansson A., Johnson T., Kaakinen M., Kapur K., Ketkar S., Knowles JW., Kraft P., Kraja AT., Lamina C, Leitzmann MF, Mcknight B, Morris AP, Ong KK, Perry JR, Peters MJ, Polasek O, Prokopenko I, Rayner NW, Ripatti S, Rivadeneira F, Robertson NR, Sanna S, Sovio U, Surakka I, Teumer A, Van Wingerden S, Vitart V, Zhao JH, Cavalcanti-Proenca C, Chines PS, Fisher E, Kulzer JR, Lecoeur C, Narisu N, Sandholt C, Scott LJ, Silander K, Stark K, Tammesoo ML, et al. 2010 Metaanalysis identifies 13 new loci associated with waist-hip ratio and reveals sexual dimorphism in the genetic basis of fat distribution. Nat Genet, 42, 949–60. [PubMed: 20935629]

Betz MJ & Enerbäck S 2017 Targeting thermogenesis in brown fat and muscle to treat obesity and metabolic disease. Nature Reviews Endocrinology, 14, 77.

Harris LA, Shew TM, Skinner JR & Wolins NE 2012 A single centrifugation method for isolating fat droplets from cells and tissues. J Lipid Res, 53, 1021–5. [PubMed: 22327205]

Suzuki T, Moriya K, Nagatoshi K, Ota Y, Ezure T, Ando E, Tsunasawa S & Utsumi T 2010 Strategy for comprehensive identification of human N-myristoylated proteins using an insect cell-free protein synthesis system. Proteomics, 10, 1780–93. [PubMed: 20213681]

Schmitt JM & Stork PJS 2000 β2-Adrenergic Receptor Activates Extracellular Signalregulated Kinases (ERKs) via the Small G Protein Rap1 and the Serine/Threonine Kinase B-Raf. Journal of Biological Chemistry, 275, 25342–25350.

Iwen KA, Backhaus J, Cassens M, Waltl M, Hedesan OC, Merkel M, Heeren J, Sina C, Rademacher L, Windjager A, Haug AR, Kiefer FW, Lehnert H & Schmid SM 2017 Cold-Induced Brown Adipose Tissue Activity Alters Plasma Fatty Acids and Improves Glucose Metabolism in Men. J Clin Endocrinol Metab, 102, 4226–4234. [PubMed: 28945846]

Hung YP, Albeck JG, Tantama M & Yellen G 2011 Imaging cytosolic NADH-NAD(+) redox state with a genetically encoded fluorescent biosensor. Cell Metab, 14, 545–54. [PubMed: 21982714]

Reers M, Smiley ST, Mottola-Hartshorn C, Chen A, Lin M & Chen LB 1995 Mitochondrial membrane potential monitored by JC-1 dye. Methods Enzymol, 260, 40617.

Salvioli S, Ardizzoni A, Franceschi C & Cossarizza A 1997 JC-1, but not DiOC6(3) or rhodamine 123, is a reliable fluorescent probe to assess delta psi changes in intact cells: implications for studies on mitochondrial functionality during apoptosis. FEBS Lett, 411, 77–82. [PubMed: 9247146]

Kriszt R, Arai S, Itoh H, Lee MH, Goralczyk AG, Ang XM, Cypess AM, White AP, Shamsi F, Xue R, Lee JY, Lee SC, Hou Y, Kitaguchi T, Sudhaharan T, Ishiwata S, Lane EB, Chang YT, Tseng YH, Suzuki M & Raghunath M 2017 Optical visualisation of thermogenesis in stimulated single-cell brown adipocytes. Sci Rep, 7, 1383. [PubMed: 28469146]

Jimenez V, Munoz S, Casana E, Mallol C, Elias I, Jambrina C, Ribera A, Ferre T, Franckhauser S & Bosch F 2013 In vivo adeno-associated viral vector-mediated genetic engineering of white and brown adipose tissue in adult mice. Diabetes, 62, 401222.

Kozak UC, Kopecky J, Teisinger J, Enerback S, Boyer B & Kozak LP 1994 An upstream enhancer regulating brown-fat-specific expression of the mitochondrial uncoupling protein gene. Mol Cell Biol, 14, 59–67. [PubMed: 8264627]

Inokuma K, Ogura-Okamatsu Y, Toda C, Kimura K, Yamashita H & Saito M 2005 Uncoupling protein 1 is necessary for norepinephrine-induced glucose utilization in brown adipose tissue. Diabetes, 54, 1385–91. [PubMed: 15855324]

Mei J, Webb S, Zhang B & Shu HB 2006 The p53-inducible apoptotic protein AMID is not required for normal development and tumor suppression. Oncogene, 25, 849–56. [PubMed: 16186796]

Wu M, Xu LG, Su T, Tian Y, Zhai Z & Shu HB 2004 AMID is a p53-inducible gene downregulated in tumors. Oncogene, 23, 6815–9. [PubMed: 15273740]

Yu XX, Lewin DA, Forrest W & Adams SH 2002 Cold elicits the simultaneous induction of fatty acid synthesis and beta-oxidation in murine brown adipose tissue: prediction from differential gene expression and confirmation in vivo. FASEB J, 16, 155–68. [PubMed: 11818363]

Barquissau V, Beuzelin D, Pisani DF, Beranger GE, Mairal A, Montagner A, Roussel B, Tavernier G, Marques MA, Moro C, Guillou H, Amri EZ & Langin D 2016 White-to-brite conversion in human adipocytes promotes metabolic reprogramming towards fatty acid anabolic and catabolic pathways. Mol Metab, 5, 352–365. [PubMed: 27110487]

Cannon B & Nedergaard J 1979 The physiological role of pyruvate carboxylation in hamster brown adipose tissue. Eur J Biochem, 94, 419–26. [PubMed: 428395]

Luttik M. a. H., Overkamp KM, Kötter P, De Vries S, Van Dijken JP & Pronk JT 1998b The Saccharomyces cerevisiae NDE1 andNDE2 Genes Encode Separate Mitochondrial NADH Dehydrogenases Catalyzing the Oxidation of Cytosolic NADH. Journal of Biological Chemistry, 273, 24529–24534.

Kajimura S, Seale P, Tomaru T, Erdjument-Bromage H, Cooper MP, Ruas JL, Chin S, Tempst P, Lazar MA & Spiegelman BM 2008 Regulation of the brown and white fat gene programs through a PRDM16/CtBP transcriptional complex. Genes Dev, 22, 1397–409. [PubMed: 18483224]

Highlights:

- Aifm2 is expressed specifically in brown adipose tissue (BAT).
- Aifm2 regenerates NAD to support robust glycolysis for thermogenesis.
- Glucose oxidation is critical for thermogenesis in fed state
- Aifm2 translocate from LD to mitochondria supports ETC for thermogenesis

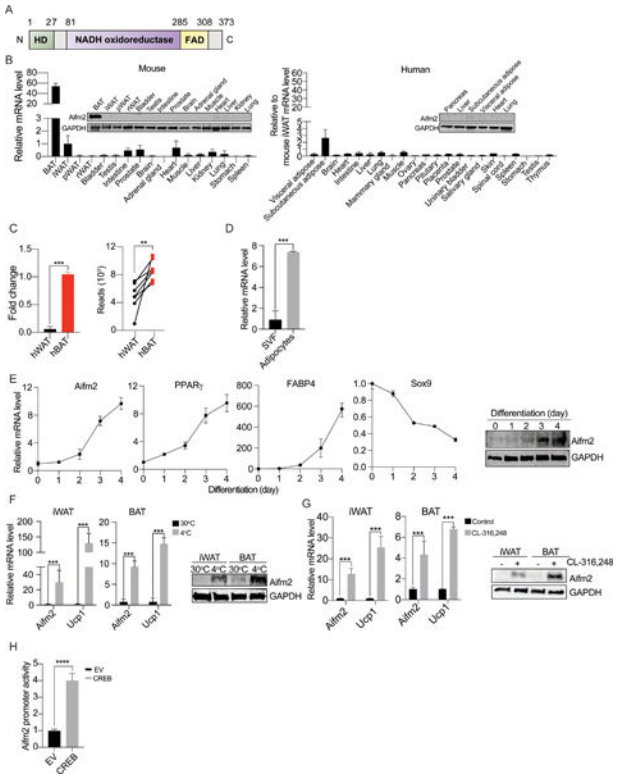

Figure 1. Aifm2 is specifically expressed in BAT and is induced by cold and β-agonist

(A) Aifm2 structure. (B) RT-qPCR/immunoblotting (IB) for Aifm2 in mouse tissues, human tissues. (C) Aifm2 expression in human BAT and WAT by microarray (left) and by RNA seq (right). (D) Aifm2 mRNA in SVF and adipocyte. (E) RT-qPCR/IB during BAT cell differentiation (n=6). (F) Aifm2 and UCP1 in iWAT and BAT of mice at 30°C or 4°C. (G) Aifm2 and UCP1 in iWAT and BAT of mice at 30°C injected with control or CL-316,248. (H) Luciferase activity using Aifm2-luc and either empty vector or CREB. Data are mean ± SD. *p<0.05, ** p< 0.01, *** p<0.001.

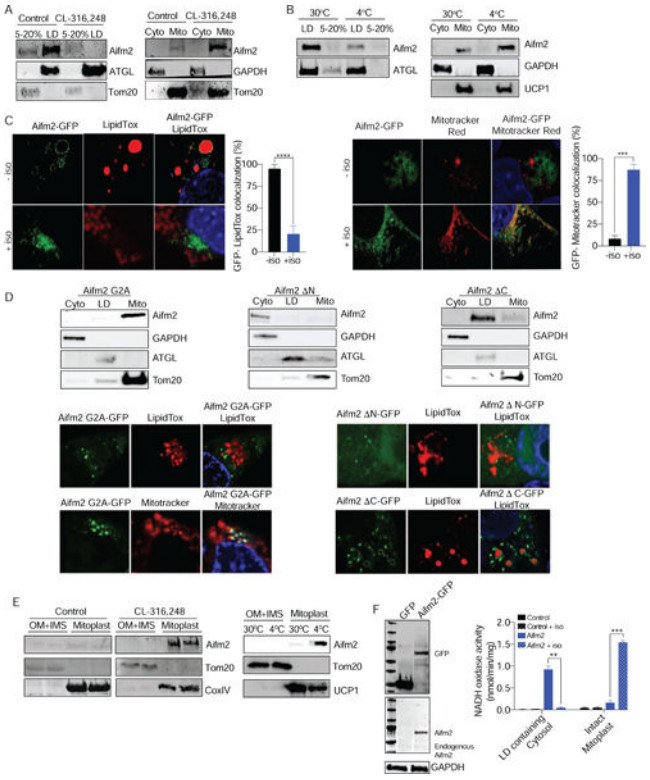

Figure 2. Aifm2 translocates from LD to mitochondria during thermogenesis.

(A) IB of indicated fraction. (B) BAT collected from mice at 30°C or 4°C and immunoblotting in indicated fraction. (C) Confocal fluorescence of Aifm2-GFP (green) in BAT cells treated in either control or isoproterenol with LD stained by LipidTOX (red) or with mitochondria stained by Mitotracker Red. (D) Localization of Aifm2 G2A mutant, Aifm2 ΔN, Aifm2 ΔC in BAT cells by IB of various fractions, and imaging of Aifm2 G2A-GFP, ΔN and (ΔC) (green) with either LipidTox or Mitrotracker Red. (E) IB in solubilized mitochondrial outer membrane and inner membrane space (OM+IMS) fraction and mitoplast fraction using BAT cells treated and BAT from mice. (F) IB for Aifm2-GFP of transfected HEK293 cells, NADH oxidase activity of Aifm2 in HEK293 by spectrophotometry at 340nm. Data are mean ± SD. *p<0.05, ** p< 0.01, *** p<0.001.

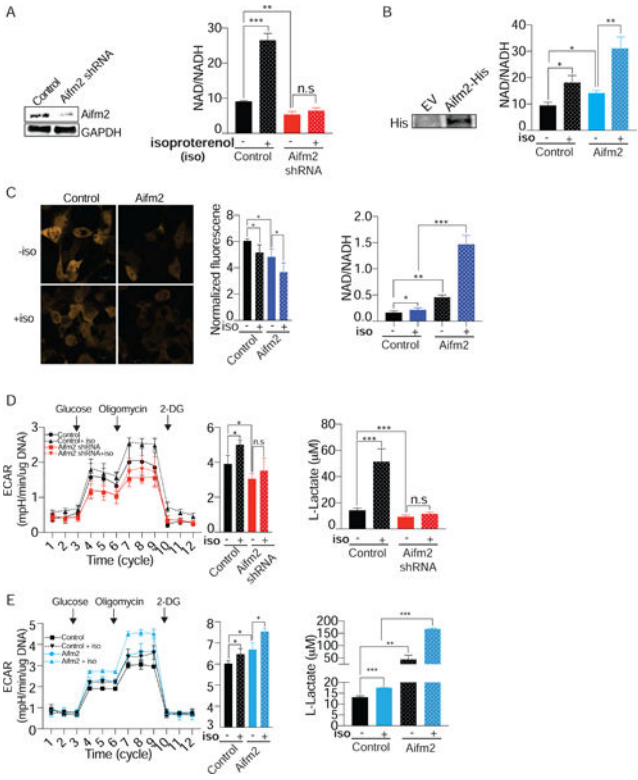

Figure 3. Aifm2 generates NAD in cytosol to increase glycolysis in BAT cells

(A) IB for Aifm2 and NAD/NADH ratio in BAT cells transduced by Aifm2 shRNA lentivirus. (B) IB for Aifm2 (left) and NAD/NADH ratio (right) in BAT cells transduced by His-Aifm2 adenovirus. (C) Fluorescence images of HEK293 cells overexpressing Peredox (green) with either Aifm2His or control vector, NADH/NAD ratio by quantification of Peredox fluorescence. (D) Extracellular acidification rate (ECAR) by XF-24 analyzer, glycolytic rate measured by ECAR under oligomycin and intracellular L-lactate concentration in Aifm2 KD in BAT cells. (E) ECAR, glycolytic rate and intracellular L-lactate in Aifm2 overexpressing BAT cells. Data are mean ± SD. *p<0.05, ** p< 0.01, *** p<0.001.

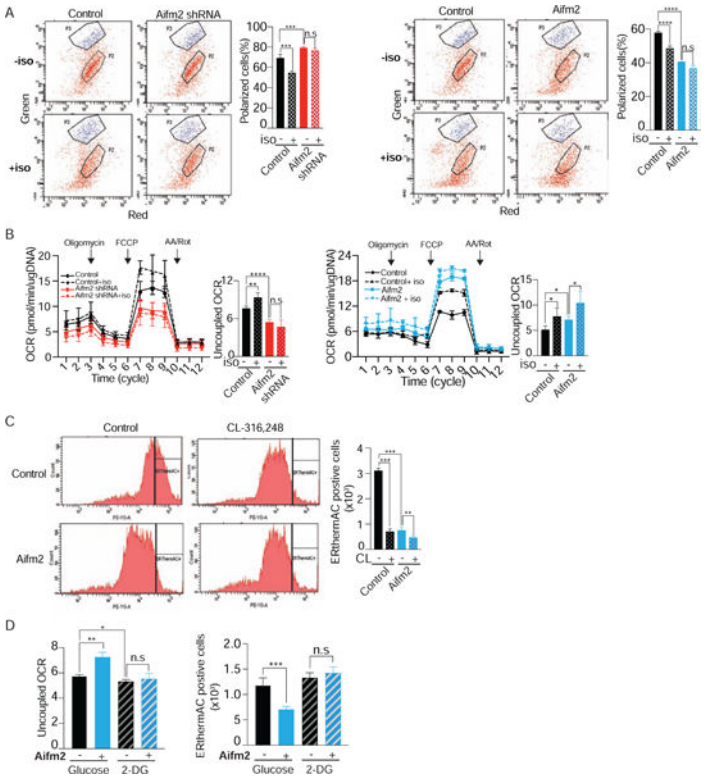

Figure 4. Aifm2 promotes thermogenesis by sustaining glycolysis in BAT cells

(A) FACS analysis of mitochondrial potential by JC-1 dye of Aifm2 KD BAT cells (left), and Aifm2 OE BAT cells. (B) OCR by Seahorse XF24 of Aifm2 KD BAT cells, and Aifm2 overexpressing BAT cells. (C) FACS analysis of ERthermAC. (D) Uncoupled OCR, and FACS analysis and quantification of ERthermAC of Aifm2 overexpressing BAT cells treated with 2 deoxyglucose. Data are mean ± SD. *p<0.05, ** p< 0.01, *** p<0.001.

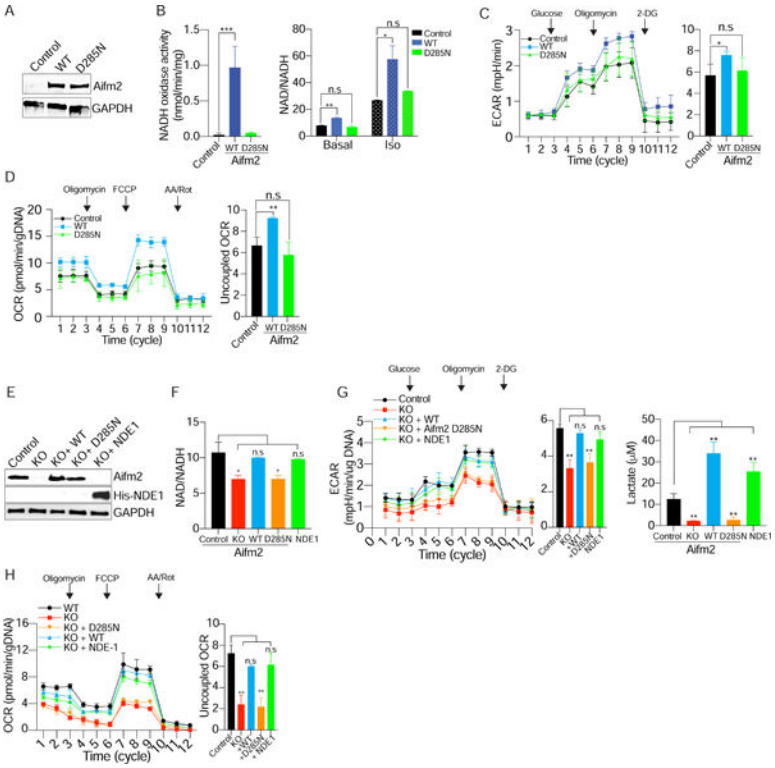

Figure 5. NADH oxidase activity of Aifm2 is required to sustain glycolysis for thermogenesis

Aifm2 WT and D285N mutant were overexpressed in BAT cells. (A) IB. (B) NADH oxidase activity of total BAT cell, and NAD/NADH ratio. (C) Extracellular acidification rate (ECAR) in BAT cells OE Aifm2 WT or D285N. (D) OCR and uncoupled OCR. Aifm2 WT and D285N mutant, and yeast NDE1 were overexpressed in Aifm2 CRISPR KO BAT cells. (E) IB. (F) NAD/NADH ratio. (G) Extracellular acidification rate (ECAR), and intracellular Llactate. (H) Total OCR and uncoupled OCR. Data are mean ± SD. *p<0.05, ** p< 0.01, *** p<0.001.

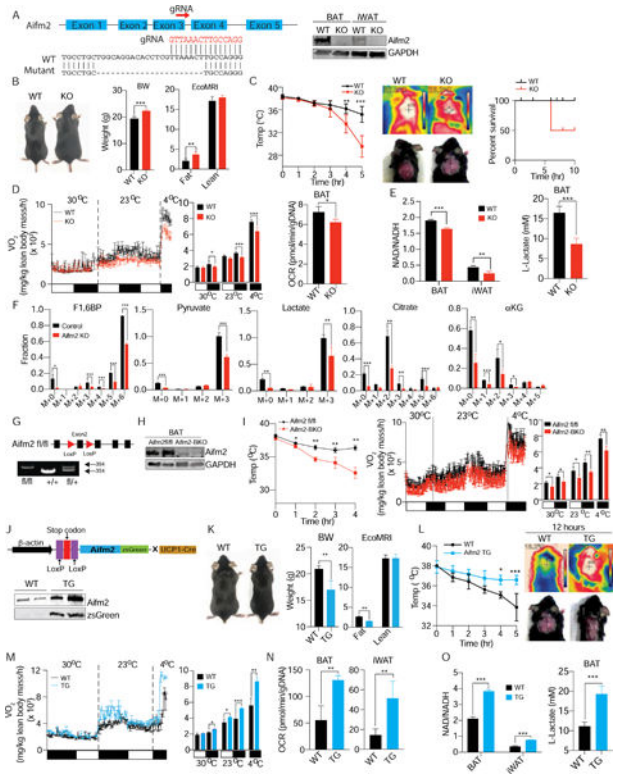

Figure 6. Aifm2 is critical for thermogenesis *in vivo*

(A) Generation of Aifm2 CRISPR KO mice and IB (B) Photograph of WT and Aifm2 KO mice, body weights and body composition. (C) Rectal temperature, infrared thermography, and survival curve of mice (n=6). (D) VO_2 by CLAMS and OCR measured in BAT from mice (n=5–7). (E) NAD/NADH measured in BAT and iWAT and intracellular L-Lactate levels in BAT (n=5–6). (F) Metabolic Flux Analysis (MFA) using [U-^{13}C] glucose. Representative glycolysis and TCA intermediates, M+1, M+2, M+3, etc. represent the number of ^{13}C atoms. (G) Generation of Aifm2 floxed mice. (H) IB for Aifm2 in BAT of Aifm2 BKO. (I) Rectal temperature, and VO_2 by CLAMS (n=5–6). (J) Generation of BAT specific Aifm2 transgenic (TG) mice. (K) Photograph of Aifm2-TG, body weights and body composition. (L) Rectal temperature and infrared thermography (n=6). (M) VO_2 by CLAMS. (N) OCR of BAT and iWAT (n=7). (O) NAD/NADH, and intracellular L-Lactate levels of BAT (n=6). Data are mean ± SD. *p<0.05, ** p< 0.01, *** p<0.001.

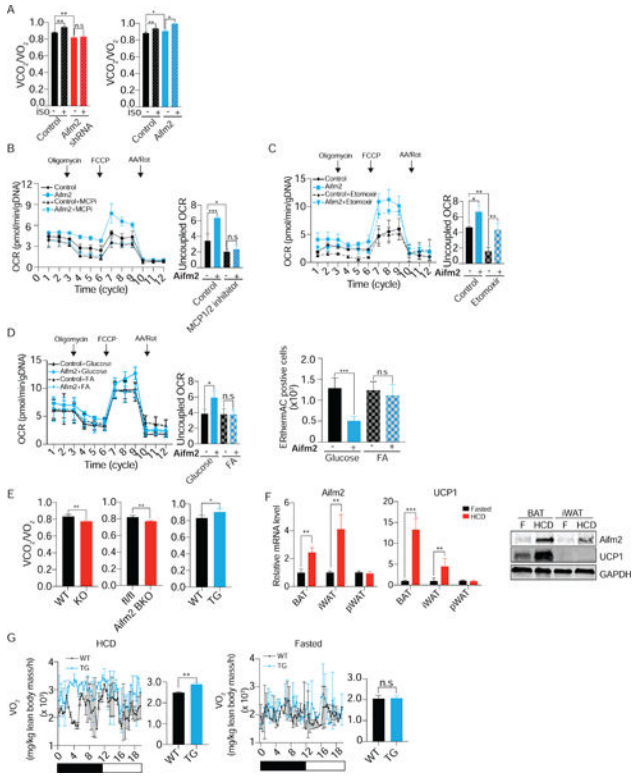

Figure 7. Aifm2 increases glucose oxidation to fuel cold/diet-induced thermogenesis

(A) V_{CO2}/V_{O2} of Aifm2 KD and OE BAT cells. (B) OCR and uncoupled OCR measured in Aifm2 overexpressing cells treated with UK5099, MCP1/2 inhibitor. (C) OCR and uncoupled OCR measured in Aifm2 OE cells treated with Etomoxir, CPT1 inhibitor. (D) OCR and uncoupled OCR, and quantification of ERthermAC positive cells of Aifm2 OE BAT cells maintained in glucose only or palmitate only containing media. (E) V_{CO2}/V_{O2} of Aifm2 KO, Aifm2 BKO and TG mice. (F) RT-qPCR/IB for Aifm2 and UCP1 in mice maintained at 30°C either fasted or fed HCD. (G) VO_2 of WT and TG mice maintained at 30°C fed HCD or fasted. Data are mean ± SD. *p<0.05, ** p< 0.01, *** p<0.001.